ACADEMIA ROMÂNĂ
*Revue Roumaine de Chimie*
http://web.icf.ro/rrch/

*Rev. Roum. Chim.*,
**2019**, *64*(12), 1019-1026
DOI: 10.33224/rrch.2019.64.12.01

# PREPARATION, CHARACTERIZATION AND MAGNETIC PROPERTIES OF $Gd_{0.8}Sr_{0.2}FeO_3$ *VIA* SOL-GEL PROCESSING

Farhang HAMEDI[a] and Haman TAVAKKOLI[b,*]

[a] Department of Chemistry, Khouzestan Science and Research Branch, Islamic Azad University, Ahvaz, Iran
[b] Department of Chemistry, Ahvaz Branch, Islamic Azad University, Ahvaz, Iran

*Received December 14, 2018*

In this paper, the nanopowders of perovskite-type $Gd_{0.8}Sr_{0.2}FeO_3$ (GSFO) were synthesized by sol–gel processing in the presence of nitrate-metal-citricacid polymer complex. These nanopowders were characterized by X-ray diffraction, scanning electron microscopy, energy dispersive X-ray spectroscopy, transmission electron microscopy and vibrating sample magnetometer (VSM) methods. XRD results showed that single perovskite phase was completely formed after calcination at 700°C. Fourier transform infrared spectra were measured for xerogel and powder sample after calcination. The TEM images showed that the average particle size of the GSFO NPs is approximately 27.65 nm and the amount of Gd, Sr, Fe, and O in GSFO was confirmed by EDX analysis. The magnetic studies also indicate that produced GSFO nanopowders exhibited ferromagnetic properties at room temperature.

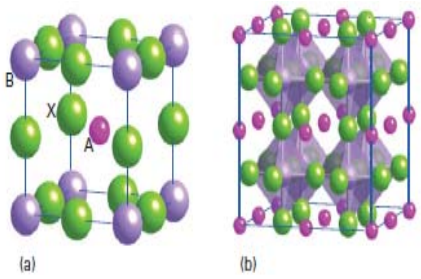


## INTRODUCTION

The mineral perovskite, $CaTiO_3$, is the structural prototype of many $ABX_3$ solids, particularly oxides. In its ideal form, the perovskite structure is cubic with each A cation surrounded by 12 X anions and each B cation surrounded by 6 anions (Fig. 1). In fact, the perovskite structure may also be described as a close-packed array of A cations and $O^{2-}$ anions with B cations in all the octahedral holes that are formed from 6 $O^{2-}$ ions, giving $B_{n/4}[AO_3]_{n/4}$ which is equivalent $ABO_3$.

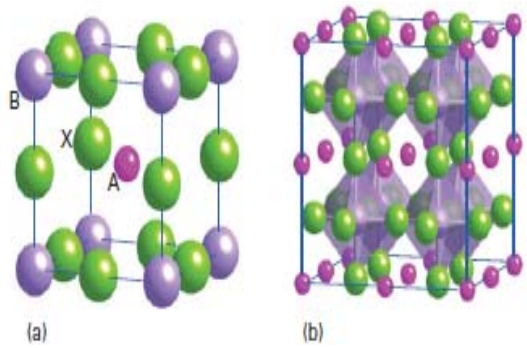


Fig. 1 – (a) The perovskite structure, $ABX_3$,
(b) a display that emphasizes the octahedral shape of the $B^-$ sites. Image taken from.[1]

* Corresponding author: e-mail: htavakkoli59@gmail.com; Tel: +98 61 34457612, Fax: +98 61 34435288

In oxides, X=O and sum of the charges A and B ions must be +6. That sum can be achieved in several ways ($A^{2+}B^{4+}$ and $A^{3+}B^{3+}$) among them, including the possibility of mixed oxides of formula $A(B_{0.5}B'_{0.5})O_3$, as in $La(Ni_{0.5}Ir_{0.5})O_3$. The A-type cation in perovskites is therefore usually a large ion (of radius greater than 110 pm) of lower charge, such as $Ba^{2+}$ or $La^{3+}$, and the B cation is a small ion (of radius less the 100 pm) of higher charge, such as $Ti^{4+}$, $Nb^{5+}$, or $Fe^{3+}$.

The perovskite structure is closely related to the materials that show interesting electrical properties, such as piezoelectricity, ferroelectricity, and high temperature superconductivity.[1] To investigate the stability of the perovskite-type compounds, $ABO_3$, Goldschmit introduced the tolerance factor (t) by the following equation:

$$t= r_A + r_O /[2(r_B + r_O)]^{1/2} \quad (1)$$

where $r_A$, $r_B$, and $r_O$ the radii of the A and B cations and oxygen ion, respectively.[2] For tolerance factors less than unity, two type of distortion from the cubic structure, the rhombohedral and orthorhombic structures, commonly occur.

Magnetic materials can be classified, or ranked, in order to their relative permeabilities; materials with permeabilities less than $\mu_0$ are diamagnets, those that are higher than $\mu_0$ are paramagnets and those with permeabilities vastly higher are ferromagnets. Superparamagnets have permeability between para-and ferro- magnets.

The permeability of a material is the ability of a magnetic field to penetrate, or permeate the medium, and is defined as the ratio:

$$\mu= B/H \quad (2)$$

while the susceptibility ($\chi$) of a material is its compliance towards magnetization, expressed as the ratio of magnetization to applied magnetic field:

$$\chi= M/H \quad (3)$$

Thus values for $\chi$ have no units. Typical susceptibility for diamagnets are of the order of negative $1 \times 10^{-6}$ and some common diamagnetic materials include Bi, Be, Ag, Au, Ge and Cu. The fact that the $\chi$ of diamagnets is negative means that they are weakly repelled by a magnetic field; their magnetic moments align anti-parallel to the applied field (in compliance with Lenz's law which attests that an induced electromotive force and the change in magnetic flux have opposing signs).

Conversely, paramagnets have positive $\chi$ value, of the order of + 0.2 to $66 \times 10^{-6}$, meaning that they are weakly attracted to a magnetic field and their atomic moments temporality align parallel with the field while it is present. Example of paramagnetic elements include β-Sn, W, Al, Pt and Mn. Ferromagnets have susceptibilities many orders of magnitude higher, and include elements such as Fe, Co, and Ni. These ideas are illustrated in Fig. 2.[4] The most stable oxidation state of lanthanoide (Ln) ions is trivalent, and the electronic configuration of $Ln^{3+}$ ions is $[Xe]4f^n$ ([Xe]: xenon electronic core). Magnetic properties of lanthanoide compounds are determined by behavior of the unpaired 4f electrons in solids. It is known that they are highly localized electrons and well shielded by the surrounding 5s and 5p electrons in the outer shell. This makes the magnetic interactions between 4f electrons in condensed matter very weak, compared with those between d electrons. In fact, many of the lanthanoid compounds are magnetically order below 4 k. One of the most challenging problems in the modern chemistry of lanthanoid compounds is to find a compound in which strong magnetic superexchange interactions between 4f electrons exist, which give rise to a long-range magnetic ordering at relatively high temperature, and to elucidate their mechanism. We have been focusing our attention on the crystal structures of the perovskite-type compounds containing lanthanoid ions.[5]

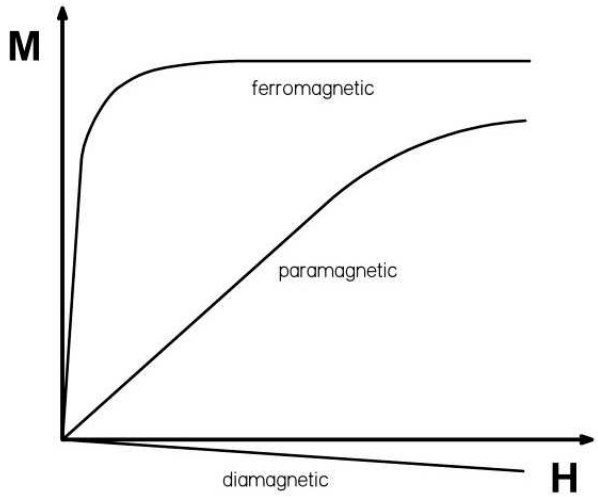


Fig. 2 – Magnetic responses, M, of ferro, para and diamagnetic materials in an applied field, H. Image taken from.[4]

The sol-gel rout synthesis is well-known to be a simple rout to get fine powders of multicompo-nents oxides with lower grain size.[6] At the

beginning, sol-gel chemistry was designed to obtain glasses[7] and ceramic materials.[8] The advantages of the sol-gel method in the preparation of mono-component materials refer to the very high purity due to the quality of the available precursors and to the possibility to tailor the textural properties of the product, especially the surface area and the pore size distribution. For the multi-component systems the following specific advantages can be mentioned: the ability to control both structure and composition at molecular level, the possibility to introduce several components in a single step, and the power to impose kinetic constraints on a system and thereby stabilize metastable phases. Furthermore, the controlled shape and size (usually, mono-disperse), and the nanometer size of the particles must be mentioned.

The objective of this work is to synthesize $Gd_{0.8}Sr_{0.2}FeO_3$ (GSFO) perovskite in the form of nanopowder by sol-gel method followed by subsequent calcination to remove any traces of organic compounds and its characterization by different techniques such as XRD, SEM-EDX, FT-IR, VSM and TEM.

## EXPERIMENTAL

### 1. Reagents

The chemicals and reagents used in this work include $Gd(NO_3)_3.\ 6H_2O$ (gadolinium nitrate-dihydrogen oxide (1/6), 99.9% purity), $Sr(NO_3)_2$ (strontium nitrate, 99.9%purity) and $Fe(NO_3)_3\ .9H_2O$ (iron (III) nitrate-dihydrogen oxide (1/9), 99.9%purity) obtained from Merck, Germany; citric acid (2-hydroxy-1,2,3-propanetricarboxylicacid, CA, 99.5% purity) was purchased from Aldrich, USA. All chemicals were analytical grade and used without further purification. The sample solutions were prepared using deionized water throughout the experiments.

### 2. Synthesis of GSFO NPs

The aqueous solution of metal nitrates (specific amounts of 3.2 mmol $Gd(NO_3)_3\ .\ 6H_2O$, 0.8 mmol $Sr(NO_3)_2$, 4 mmol $Fe(NO_3)_3\ .\ 9H_2O$) with nominal atomic ratios Gd : Sr : Fe : O = 0.8: 0.2: 1: 3, were mixed together in 40 mL deionized water. Then, citric acid (16 mmol) was added slowly to the metal solution at room temperature under the constant magnetic stirring (1000 rpm). The initially clear solution obtained a transparent brown coloration after adding CA. The solution pH is adjusted under 7(acidic pH) with ammonia (0.5 $mol.L^{-1}$) and nitric acid (1 $mol.L^{-1}$) solutions. The solution was refluxed at approximately 160°C with stirring for 60 min to convert it to a stable complex. To make a gel, stirring was continued at 170°C for 135 min. During the evaporation of the solvent, a reddish-brown gas corresponding to $N_xO_y$ comes out of the solution. This $N_xO_y$ departure occurs mostly at the end of evaporation and is very exothermic. The dry gel was obtained by letting the wet gel into oven and heated slowly up to 110°C and kept for 14 h in a baking oven. The gel was ground in an agate mortar and turned into powder. Then, GSFO nanopowder was obtained by calcination of the precursors at 700°C for 6 h in electrical furnace. The annealing of the amorphous precursor at 700°C allows to remove the residual carbon, and to obtain the orthorhombic perovskite phase.

The word equation of this process is given below:
Gadolinium nitrate hexa hydrate + Strontium nitrate + Iron (III) nitrate nona hydrate + Citric acid → viscose gel → Products

### 3. Characterization

Several techniques were employed to analyze and validate the synthesized powder. For structural investigation of calcined powder at 700°C XRD measurements were carried out in the region of ($2\theta$ = 20 to 80°) using Cu-$K_\alpha$ radiation on a Equinox 3000 INEL XRD diffractometer equipped with a curved germanium monochromator. The microstructure of powder was examined using Zeiss-EM10C TEM under a working voltage of 80 kV, while the morphology and chemical analysis of the particles was investigated using SEM-EDX (MIRA 3, 15.0kV, Czech) techniques. Measurements of the magnetic moment were carried out in a VSM MDKFD, Iran magnetometer in a range of -10KOe to 10 KOe at 298 K. The FT-IR transmission spectra in the region 400-4000 $cm^{-1}$ were recorded for sample using FT-IR PerkinElmer BX II, USA by KBr pellet technique.

## RESULTS AND DISCUSSION

### 1. Microscopic analyses

Figure 3 shows typical TEM images of nanosized GSFO calcined at 700°C prepared by the modified sol-gel method. The powder was characterized by nano-bars type particles and particles size distribution appears to be good. The size of NPs of GSFO sample is in the range of 18 to 38 nm. This value is in agreement with the result achieved from XRD measurement.

Based on the SEM images, the surface looks rough and nearly fully covered with the particles grown on it. SEM image of GSFO showed an uniform grain size distribution, a fine powder size, and homogenous nanostructure for the material obtained by sol-gel method. The mean particle size is within the nanoscale (< 100 nm) (Fig. 4). This value is in accordance with the result obtained by the measurement of XRD peak broadening.

EDX analysis was used to determine the composition of the sample. It shows peaks corresponding to gadolinium, strontium, iron and oxygen in the spectrum Fig.5. It means that no impurities could be seen within the detection limit of the EDX. The result of quantitative analysis from the spectra is presented in the table 1. The quantitative analysis is consistent with the synthesis condition.

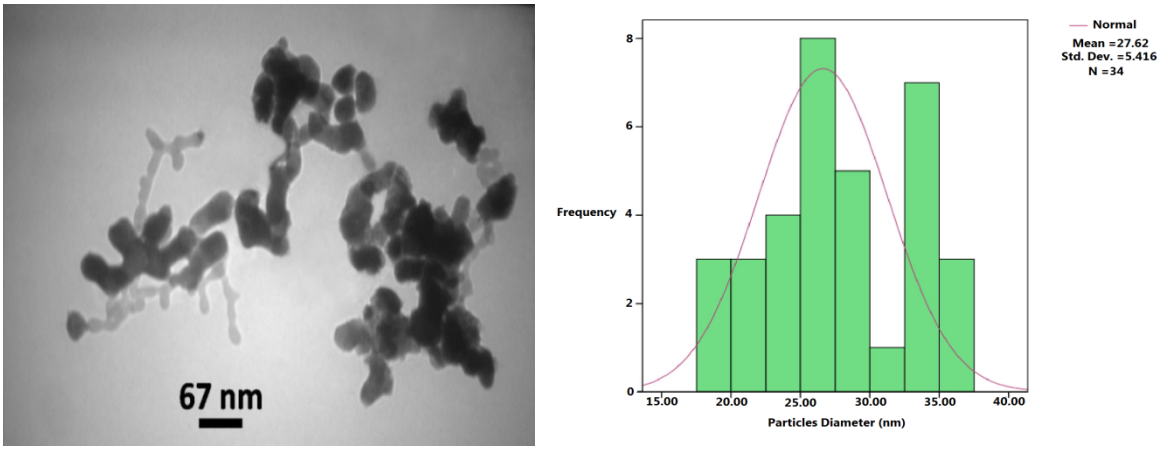


Fig. 3 – (a) TEM image and (b) calculated histogram of the GSFO nanopowder obtained at 700°C.

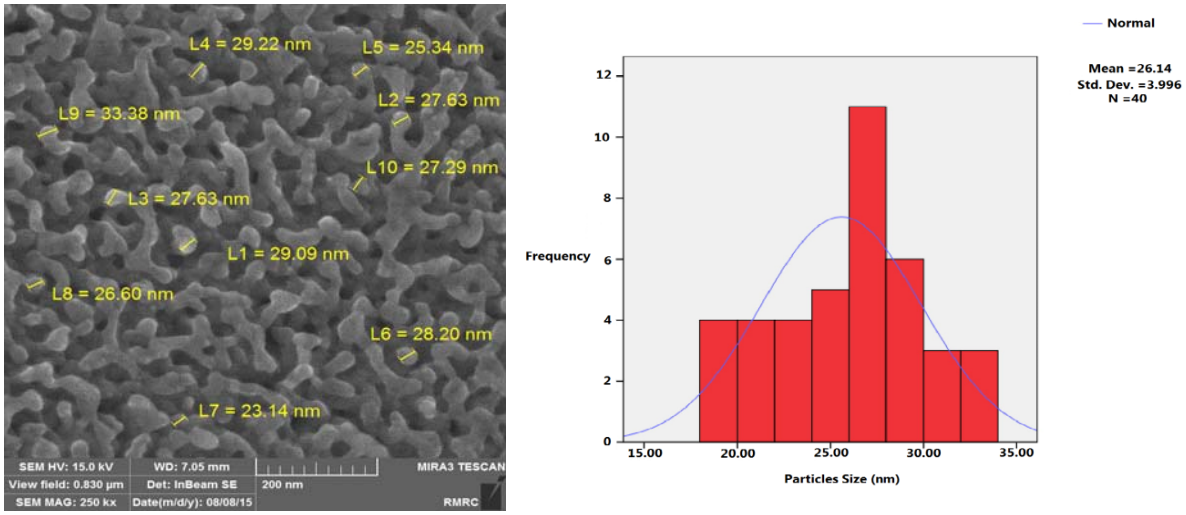


Fig. 4 – (a) SEM image and (b) particle size distribution histogram for dried xerogel of the GSFO nanoparticles.

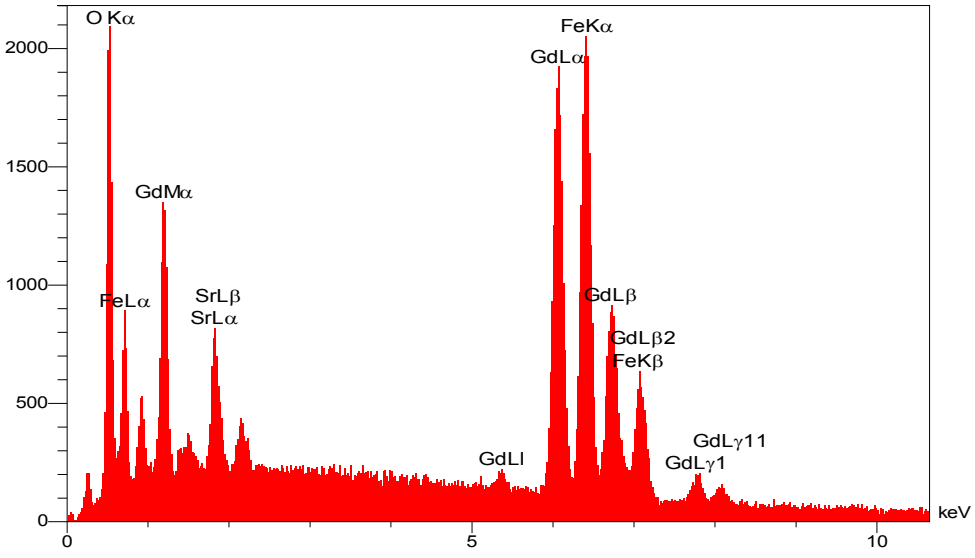


Fig. 5 – EDX result of the GSFO NPs.

*Table 1*

EDX element composition analysis of GSFO NPs

| Elt | Line | W % | A % |
|---|---|---|---|
| Gd | Lα | 50.34±1.51 | 14.52±0.44 |
| Sr | Lα | 6.98±0.21 | 2.15±0.06 |
| Fe | Kα | 22.33±0.89 | 15.42±0.62 |
| O | Kα | 19.35±0.39 | 67.91±1.36 |

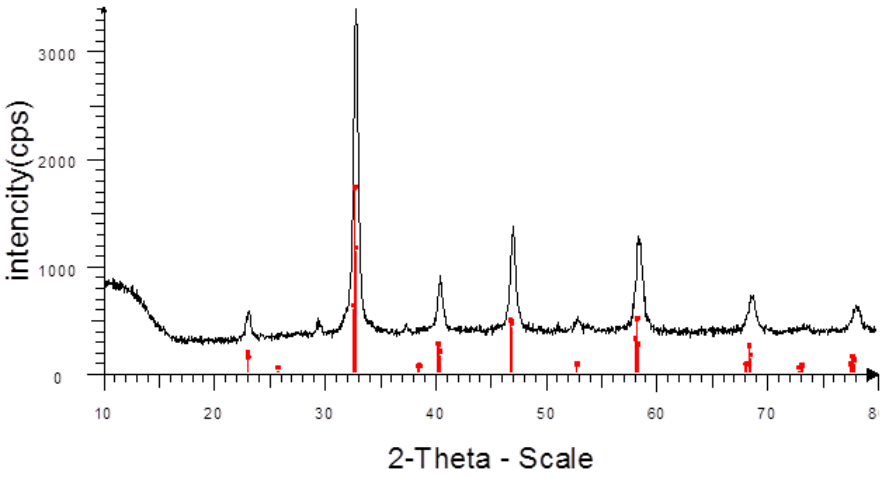


Fig. 6 – X-Ray diffraction patterns of the GSFO nanopowder calcined at 700°C.

## 2. X-ray diffraction analysis

XRD analysis has been made on GSFO calcined at 700°C for 6 h in electrical furnace. XRD shows that sample is single phase with no detectable secondary phases and this sample can be indexed with monoclinic structure with the space group F (0). The crystallite size, $D_{hkl}$, of the sample prepared at 700°C to the peak at 2θ=33.1° was calculated from the main reflection of the orthorhombic-distorted perovskite by means of the Debye-Scherrer equation:

(7)

where $k$ is a shape factor which normally ranges between 0.9 and 1.0(in our case, $k$ = 0.9), λ the X-Ray wavelength (Cu-Kα, λ= 1.54060Å), $\beta_{hkl}$ is the peak width of half-maximum, and $\theta_{hkl}$ (rad) is the Bragg angle of (hkl) peak.[9-11] Very sharp and strong peak indicates a very good crystallization of the product. The average crystallite size of GSFO NPs was approximately 22.20 nm.

In this Fig.6, we can identify the presence of (002), (202), (222), (004), (224), (404), and (206) crystal planes of metallic monoclinic structure for GSFO (Ref. Code: ICDD-00-047-0067). The diffraction peaks at 2θ angles appear at 23.2°, 32.5°, 41°, 47.1°, 58.5°, 68.4°, and 78.1°.

## 3. FT-IR analysis

The FT-IR spectra of the GSFO fresh xerogel and annealed xerogel in the range 400-4000 $cm^{-1}$ were shown in Fig. 7. The FT-IR spectrum is similar to the most other $ABO_3$-type perovskite compounds which have common $BO_6$ oxygen-octahedral structure.[12-14] The sample showed the typical M-O-C pair vibrations around 1387.94 and 1619.07 $cm^{-1}$.[15] In general, lattice water absorbs at 3550-3200 $cm^{-1}$ (in this paper: 3414.19 $cm^{-1}$) (antisymmetric and symmetric OH stretchings) and at 1630-1600 $cm^{-1}$ (in this study: 1619.06 $cm^{-1}$) (H-O-H bending) in agreement with Nakamoto.[16] In agreement with the literature data, the bands in the range of 1300-

1200 $cm^{-1}$ (in this study: 1220.40 $cm^{-1}$) correspond to ν C-O from –COOH group of the citric acid.[17] The bands at about 1719.84 $cm^{-1}$ and 1387.94 $cm^{-1}$ are due to $\nu_{as}$ ($COO^-$) and $\nu_{sym}$ ($COO^-$), respectively. On the other hands, the band at about 1072.39 $cm^{-1}$ corresponds to π (CH) /π (COO).[17] According to Deacond, this value shows that the carboxylic group of the citrate ligands act of bridging ligands.[17,18] The band from 1021.97 $cm^{-1}$ corresponds to the $\nu_2$ ($NO_3^-$)/ρ($CH_3$ ).[17] The bands correspond to O-H group, $NO_3^-$ and carboxylate impurities disappear as the gel was annealed at 700°C. Several broad bands are observed at 400-900 $cm^{-1}$ in the IR spectra of GSFO, one of them is strong at 858.83 $cm^{-1}$ and other weak peaks at 575.38 and 437.32 $cm^{-1}$. These peaks are characteristic of perovskite oxides and can be attributed to νM-O stretching and δO-M-O bending mode of vibrations, respectively.[19-21] These observed infrared peaks belong to $\nu_1$-$BO_6$ (B=Fe) stretching normal modes along the spontaneous polarization vibration in these structure.[22]

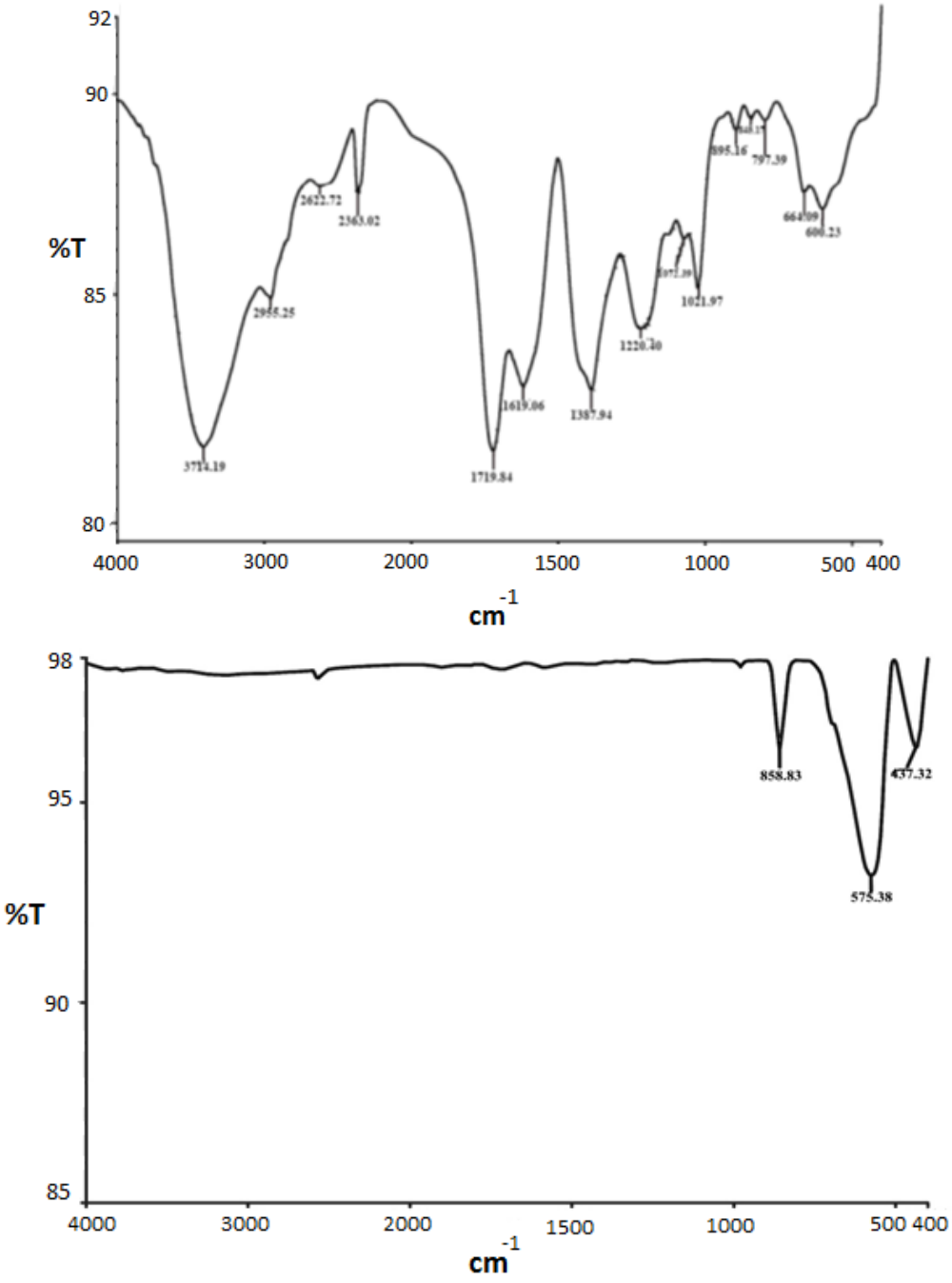


Fig. 7 – FT-IR spectra of the GSFO (a) fresh xerogel, (b) the calcined powders at 700°C for 6 h in electrical furnace.

## 4. Magnetic properties analysis

VSM technique was employed to study magnetic properties of synthesized GSFO NPs at room temperature, whose resultant magnetization curve is shown in Fig 8. The magnetization curve indicates magnetization as a function of applied magnetic field. Based on this curve, data related to coercivity field ($H_c$), remanent magnetization ($M_r$), saturation magnetization ($M_s$) as the magnetic characterization of sample were calculated whose obtained results consist of $M_s$ = 7.05654 emu/g, $M_r$ = 3.39213 emu/g, $H_c$ = 783.88 Oe and $M_r/M_s$ = 0.48. From magnetic measurements can be observed that the sample is hard ferromagnetic material.[23-26] Magnetic properties of various perovskite materials have been studied by the researchers' worldwide. Such as: Pawar and coworker used the $Ni_{0.5}Co_{0.5}Gd_yFe_{2-y}O_4$ (y = 0.025) nanocrystalline were prepared using modified sol-gel route. The magnetic parameters of this sample are: $M_s$ = 29.74 (emu/g), $M_r$ = 21.37 (emu/g) and $H_c$ = 12.88 (Oc).[27] All parameters show increased values as compared to bulk Gd doped $Ni_{0.5}Co_{0.5}Fe_2O_4$ ferrite sample. On the other hand, Praveena *et al.* have synthesized the $Y_{3-x}Gd_xFe_5O_{12}$ (X = 0.00, 0.05, 0.15 and 0.25) NPs via sol-gel method and magnetic properties of all the samples are presented in Table 3.[28]

The magnetic moments of rare-earth ions generally originate from localized 4f electrons and these are characterized by lower magnetic ordering temperatures.[29] Therefore their magnetic dipolar orientation exhibits a disordered form at room temperature and hence $Gd^{3+}$ ions can be considered as nonmagnetic and make no contribution to the magnetization of doped ferrite at room temperature.[30] Hence the obtained results in this work, are in good agreement with reported literature.[27,28]

## CONCLUSIONS

The NPs 0f $Gd_{0.8}Sr_{0.2}FeO_3$ was synthesized by the improved conventional sol-gel processing using CA as a complexing reagent followed by the obtained sample sintering at 700°C for 6 hours. The phase of the as-prepared product is identified by XRD. The line width analysis is consistent with an average crystalline size of ~22 nm with monoclinic structure for GSFO. The SEM-EDX and TEM methods were employed to characterize the morphology and composition of this nanomaterial. The IR spectra revealed that $CO_3^{2-}$ and $NO_3^-$ ions presented on the sample surface disappear during heat treatment. The magnetic susceptibility indicates the presence of ferromagnetic behavior in the system.

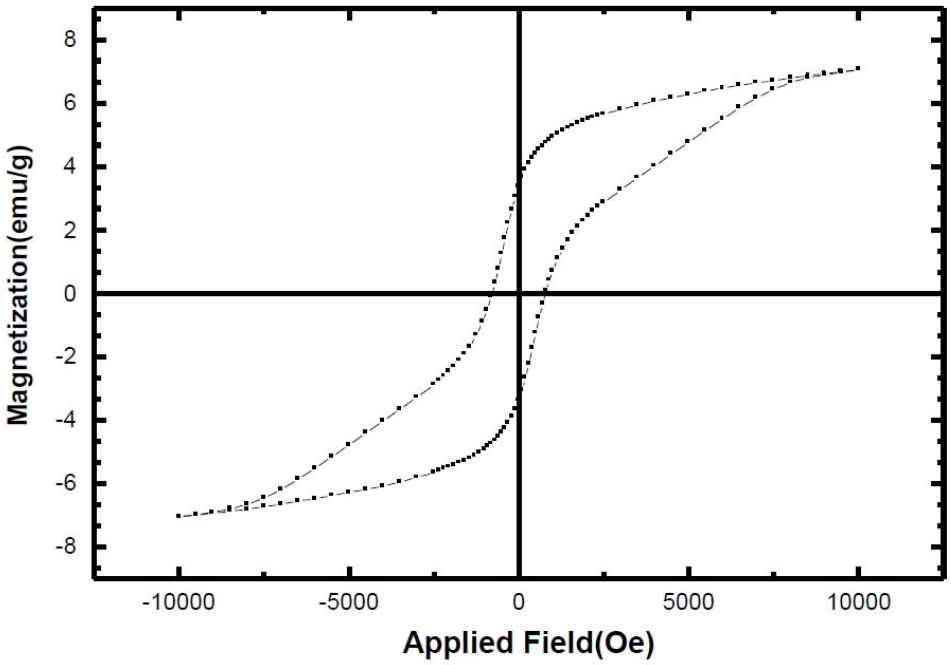


Fig. 8 – Magnetic curve of the GSFO NPs at 298 K. Inset: the enlarge curve from -10 to 10 KOe.

*Table 2*

Magnetic parameters of $Y_{3-x}Gd_xFe_5O_{12}$ (X = 0.00, 0.05, 0.15 and 0.25) NPs

| Composition(x) | $M_s$ ($Am^2/Kg$) | $M_r$ ($Am^2/Kg$) | $H_c$ (mT) |
|---|---|---|---|
| 0 | 25 | 13.6 | 27 |
| 0.05 | 20 | 8 | 36 |
| 0.15 | 16 | 4.6 | 42 |
| 0.25 | 13 | 1.7 | 54 |

## REFERENCES


1. P. Atkins, T. Overton, J. Rourke, M. Weller and M. Hagerman, "Inorganic Chemistry", fifth edition, Oxford University Press, Great Britain, 2010.
2. P. M. Woodward, *Acta Crystall. B*., **1997**, *53*, 44-66.
3. K. Tezuka, Y. Hinatso, A. Nakamura, T. Inami, Y. Shimojo and Y. Morii, *J. Solid State Chem*., **1998**, *141***,** 404-410.
4. D. C. Tonkin, "Characterization of Magnetic Nanoparticles and their evaluation for use in Hyperthermia studies", RMIT University, 2014.
5. Y. Hinatso, Y. Izumiyama, Y. Doi, A. Alemi, M. Wakeshima, A. Nakamura and Y. Morii, *J. Solid State Chem*., **2004**, *177*, 38-44.
6. M. Crisan, *Rev. Roum. Chim.,* **2018**, *63*, 385-392
7. S. Sakka, *Bull. Inst. Chem. Res., Kyoto Univ.,* **1983**, *61*, 376-396.
8. P. Colomban*, Ceram. Int*., **1989**, *15*, 23 - 50.
9. H. Tavakkoli and M. Yazdanbakhsh, *Microporous and Mesoporous Mater*., **2013**, *176***,** 86-94.
10. N. A. Merino, B. P. Barbero, P. Ruiz and L. E. Cadu, *J. Catal.,* **2006**, *240*, 245-257.
11. F. Bin, C. Song, G. Lv, J. Song, C. Gong and Q. Huang, *Ind. Eng. Chem. Res*., **2011**, *50*, 6660-6667.
12. E. R. Leite, C. M. G. Sousa, E. Longoand and J. A. Varela, *Cream. Int*., **1995**, *21*, 143-152.
13. W. Nimmo, N. J. Ali, R. M. Brydson, C. Calvert, E. Hampartsoumian, D. Hind and S. J. Milne, *J. Am. Cream. Soc*., **2003**, *86*, 1474-1480.
14. A. Sakar-Deliormanl, E. Celik and M. Pola, *Cream. Int.,* **2009**, *35***,** 503-508.
15. J. Kim and I. Honma, *Electrochim. Acta*., **2004**, *49*, 3179-3183.
16. K. Nakamoto, "Infrared and Raman Spectra of Inorganic and Coordination Compounds", Part B., "Applications in Coordination, Organometallic and Bioinorganic Chemistry", 6th Edition, John Wiley & Sons Inc., New York, 2009.
17. L. Predoana, A. Jitianu, B. Malic and M. Zaharescu, *J. Am. Ceram. Soc*., **2012**, *95*, 1068–1076.
18. G. B. Deacon and R. J. Phillips, *Coord. Chem. Rev*., **1980**, *33*, 227–50.
19. D. A. Neumayer and E. Cartier, *J. Appl. Phys*., **2001**, *90*, 1801-1808.
20. Y. Hao, J. Li, X. Yang, X. Wang and L. Lu, *Mater. Sci. Eng. A*., **2004**, *367*, 243-247.
21. R. N. Singh and B. Lal, *Int. J. Hydrogen Energy*., **2000**, *27*, 45-55.
22. M. Yazdanbakhsh, H. Tavakkoli and S. M. Hosseini, *S. Afr. J. Chem*., **2011**, *64*, 71-78.
23. S. P. Altintas, A. Amira, A. Varilci and C. Terzioglu, *J. Magn. Magn. Mater.,* **2012**, *324*, 1331-1336.
24. N. Dhahri, A. Dhahri, J. Dhahri, E. K. Hlil and E. Dhahri, *J. Magn. Magn. Mater*., **2013**, *326*, 129-137.
25. J. W. Wilson, N. Karimian, J. Liu, W. Yin, C. L. Davis and A. J. Peyton, *J. Magn. Magn. Mater.,* **2014**, *360*, 52-58.
26. T. R. Gopalarao, S. Ravi and D. Pamu, *J. Magn. Magn. Mater*., **2016**, *409*, 148-154.
27. D. B. Pawar and L. S. Ravangave, *J. Appl. Phys.,* **2019**, *11*, 42-44.
28. K. Praveena and S. Srinath, *J. Magn. Magn. Mater*., **2014**, *349*, 45-50.
29. W. J. Nellis and S. Legvold, *Physical Review*, **1969**, *180*, 581–590.
30. J. Jing, L. Liangchao and X. Feng, *J. Rare. Earth.*, **2007**, *25*, 79–83.